Published OnlineFirst July 14, 2010; DOI:10.1158/0008-5472.CAN-10-0184

Construction of reporter and expression vectors

The 5′ flanking region of mouse *TfR1* (from bp +16 to +436; +1 indicates the transcription start site) gene was amplified using Elongase Enzyme mix (Invitrogen) using DNA extracted from Colon 26 cells. PCR was performed using the forward primer 5′-AGTTGAGCTC(*SacI*)GGCTTGGTGCAGCTCAGTTAGTAG-3′ and reverse primer 5′-ATGAGATATC(*Eco*RV)TAAATGTCCGTTGACACTAGTAACC-3′. The PCR products were purified and ligated into a pGL4 Basic vector (*TfR*1-Luc). The sequence of the CACGTG E-box (bp +290 to +295) on *TfR*1-Luc was mutated using a QuikChange site-directed mutagenesis kit (Stratagene). Expression vectors for mouse CLOCK, BMAL1, and c-Myc were constructed using cDNAs obtained from RT-PCR derived from mouse liver RNA. All coding regions were ligated into the pcDNA3.1 (+) vector (Invitrogen), as previously described (7). Protein expression levels from each expression vector in Colon 26 were assessed by Western blotting analysis (Supplementary Data S2).

Luciferase reporter assay

Colon 26 cells were seeded at 3×10^5 cells per well in six-well culture plates (BD Biosciences). After an 18-hour culture, the cells were transfected with 100 ng per well of reporter vector and 2 μg per well (total) of expression vector using Lipofectamine LTX reagent (Invitrogen). A 0.5-ng-per-well sample of phRL-TK vector (Promega) was also cotransfected as an internal control reporter. The total amount of DNA per well was adjusted by adding pcDNA3.1 vector (Invitrogen). At 24 hours posttransfection, cells were harvested and the cell lysate was analyzed using a dual-luciferase reporter assay system (Promega). The ratio of firefly luciferase activity to *Renilla* luciferase activity in each sample served as a measure of normalized luciferase activity.

Small interfering RNA

siRNA of the mouse *c-Myc* gene was designed using BLOCK-iT RNAi Designer (Invitrogen). The siRNA oligonucleotide sequences were as follows: siRNA control sense, 5′-UAGUGUGAGCACUGUGAUUCCUUGG-3′ and antisense 5′-CCAAGGAUCACAGUGCUCACACUA-3′; *c-Myc* siRNA sense 5′-UAGUCGAGGUC-AUAGUUCCUGUUGG-3′ and antisense 5′-CCAACAGGAACUAUGACCUCGACUA-3′. The oligonucleotides were transfected into Colon 26 cells at a final concentration of 20 nmol/L using Lipofectamine 2000 (Invitrogen).

Chromatin immunoprecipitation assays

Tumor masses were excised and treated with 1% formaldehyde for 5 minutes at room temperature to cross-link the chromatin, and the reaction was stopped by adding glycine to a final concentration of 0.125 mol/L. Each cross-linked sample was sonicated on ice and then incubated with antibodies against c-MYC, CLOCK, rabbit-IgG, or goat-IgG (Santa Cruz Biotechnology). Chromatin/antibody complexes were extracted using a protein G agarose kit (Roche). DNA was isolated using the Wizard SV Genomic DNA Purification System (Promega) and subjected to PCR using the following primers for the c-MYC binding site (E-box) of the *TfR1* promoter region, forward 5′-GTGACTCCCTTGTCAG-3′ and reverse 5′-CCGTGACACTAGTAACC-3′. For PCR analysis, PCR products were amplified for 40 or 45 cycles. PCR products were run on an agarose (3%) gel, including 0.2 μg/mL ethidium bromide, and analyzed using the NIH image software.

Determination of L-OHP (Pt) concentration

Plasma samples were obtained by centrifugation at 3,000 rpm for 3 minutes and stored at −20°C until analysis. Tumor DNA was extracted using a Wizard Genomic DNA Purification kit (Promega). Measurements of the L-OHP (Pt) content in plasma and tumor DNA were made using ICP-MS at the Center of Advanced Instrumental Analysis, Kyushu University. ICP-MS is capable of detecting very small amounts of Pt. Plasma Pt concentration and its tumor DNA content were expressed as micrograms per milliliter and nanograms per nanogram of DNA, respectively.

Determination of the antitumor effect

Seven days after the inoculation of Colon 26 cells into mice, a single injection of Tf-NGPE L-OHP (L-OHP: 0, 7.5 mg/kg, i.v.) or vehicle (9% sucrose) was given to tumor-bearing mice at 9:00 a.m. or 9:00 p.m. This dosage of Tf-NGPE L-OHP was selected based on a preliminary study (Supplementary Data S3). In all mice, the tumor volumes were measured every 3 days throughout the duration of the experiment.

Statistical analysis

ANOVA was used for multiple comparisons, and Scheffe's test was used for comparison between two groups. A 5% level of probability was considered significant.

Results

Twenty-four-hour rhythm in the expression of TfR1 in Colon 26 tumor masses

Two subtypes of TfR have been identified: TfR1 and TfR2. In implanted Colon 26 cells, *TfR1* but not *TfR2* was detectable, although *TfR2* was expressed in mouse liver (Supplementary Data S1B). The protein and mRNA levels of TfR1 in implanted Colon 26 cells showed a significant 24-hour rhythm, with higher levels during the early dark phase ($P < 0.05$; Fig. 1A and B). The increase and decrease in mRNA levels of *TfR1* seemed to cause the rhythm of TfR1 protein in Colon 26 tumor masses.

Regulation of the 24-hour rhythm in the expression of *TfR1* gene by c-MYC

Among these, c-MYC is a potent activator of *TfR1* gene transcription in mice and humans, and the transactivation effect was elicited through binding to the CACGTG E-box located in the first intron region (18, 19). In addition, CLOCK/BMAL1 heterodimers also bind cooperatively to CACGTG E-box sequences and regulate the rhythmic expression of their target genes (2). Thus, to establish the relevance of the biological clock system on the expression of *TfR1*, CLOCKΔ19 (CLOCK protein lacking transcriptional activity) was overexpressed in Colon 26 cells. Clock mutant mice have

Published OnlineFirst July 14, 2010; DOI:10.1158/0008-5472.CAN-10-0184

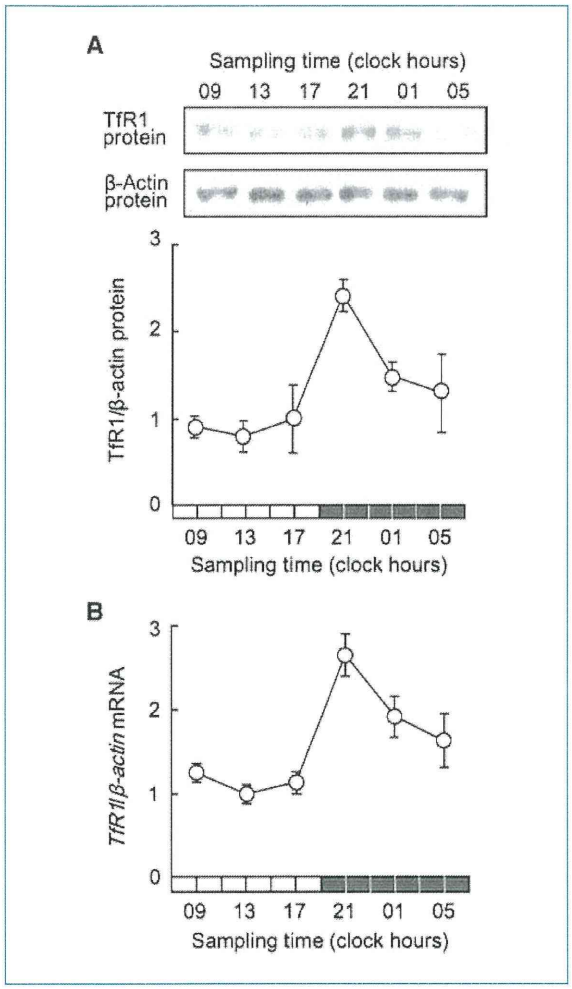

Figure 1. Twenty-four hour variation in the expression of TfR1 in Colon 26 tumor masses. A, temporal expression profile of TfR1 protein in tumor masses. The photographs show 24-h variation in TfR1 protein in implanted Colon 26 tumor cells. Cytoplasmic proteins were measured using each of the antibodies. Bottom, relative TfR1 protein levels. The data were normalized using β-actin as a control. Points, mean (n = 3, P < 0.01, ANOVA); bars, SEM. B, temporal expression profile of *TfR1* mRNA in tumor masses. The data are normalized using β-*actin* as a control. Points, mean (n = 6, P < 0.01, ANOVA); bars, SEM.

a point mutation in exon 19 of the *Clock* gene and exhibit low-amplitude rhythms in the expression of various genes (20). *TfR1* and *c-Myc* expression levels were low in CLOCKΔ19 overexpressing Colon 26 cells (Supplementary Data S4). Next, we tested whether these transcription factors participate in regulation of the rhythmic expression of *TfR1* gene in Colon 26 cells. Cotransfection of *TfR1*-Luc with c-MYC expression constructs resulted in an 8.1-fold increase in promoter activity, whereas CLOCK/BMAL1 had little effect on the transcriptional activity of the *TfR1* gene (Fig. 2B). The transactivation effect of c-MYC on *TfR1* reporters was dependent on the E-box element located from bp +290 to +295 because mutation of the CACGTG sequence to AAGCTT reduced transcriptional activation by c-MYC from 8.1- to 1.5-fold.

Several compounds and high concentration serum have been shown to induce and/or synchronize circadian gene expression in cultured cells (21). Thus, to elucidate the role of c-MYC in the circadian regulation of *TfR1* expression, the temporal expression profiles of *TfR1* mRNA in c-MYC–downregulated Colon 26 cells were investigated after 50% FBS treatment. Brief exposure of control scrambled siRNA-transfected cells to 50% FBS resulted in the oscillation of *TfR1* mRNA levels with a period length of ~24 hours (Fig. 3A). On the other hand, the protein levels of c-MYC were decreased and the mRNA levels of *TfR1* failed to show a significant 24-hour oscillation after the treatment of *c-Myc* siRNA–transfected cells with 50% FBS (Fig. 3B and C). These results suggested that c-MYC is required for generating the time-dependent variation in *TfR1* mRNA expression.

The transcription of *c-Myc* is regulated by components of the circadian clock, and its mRNA levels in mouse liver and bones have been shown to exhibit a significant 24-hour oscillation (22). The protein levels of c-MYC in Colon 26 cells implanted in mice also showed obvious 24-hour oscillations with higher levels around the early dark phase and lower levels during the early light phase, whereas there was no obvious 24-hour variation in the protein levels of CLOCK in the tumor

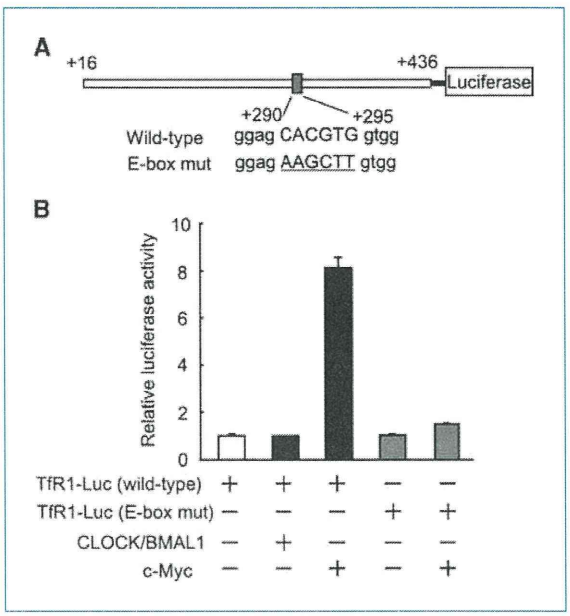

Figure 2. Influence of CLOCK/BMAL1 and c-MYC on transcription of the mouse *TfR1* gene. A, schematic representation of the mouse *TfR1* promoter. The numbers on both sites, the distance (bp) from the transcription start site (+1) included in the luciferase reporter construction. The numbers of nucleotide residues below the box, the positions of the E-box. The underlined nucleotide residues, the mutated sequence of the E-box. B, wild-type or E-box–mutated *TfR1* gene reporter plasmids (*TfR1*-Luc) were cotransfected with expression constructs encoding CLOCK/BMAL1 or c-MYC. Columns, mean (n = 3); bars, SEM.

Published OnlineFirst July 14, 2010; DOI:10.1158/0008-5472.CAN-10-0184

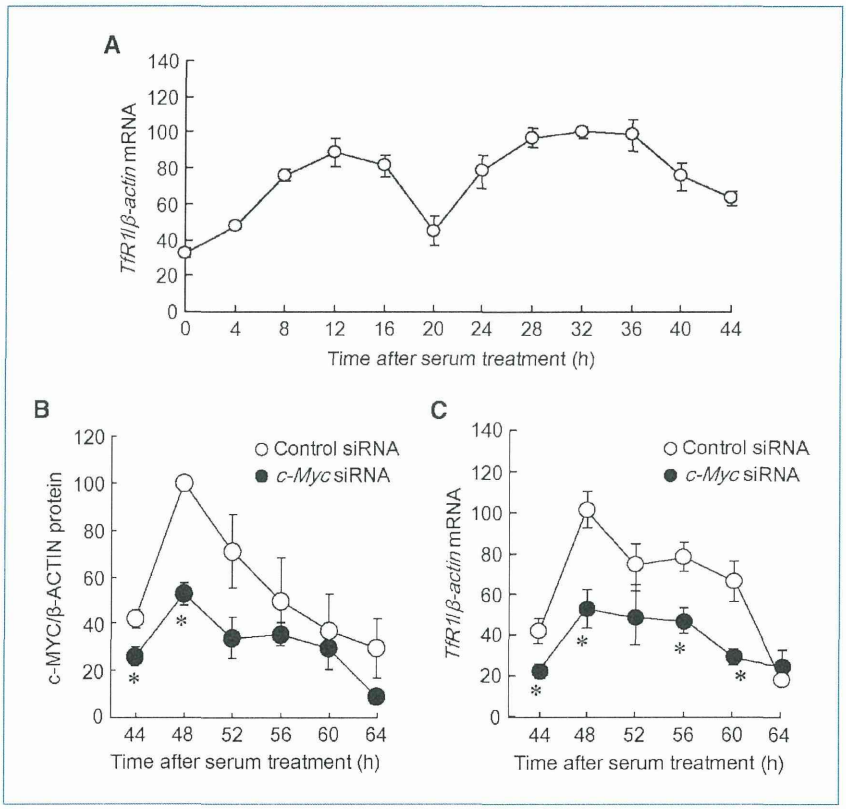

Figure 3. Influence of the downregulation of c-MYC on the rhythmic expression of *TfR1* mRNA in Colon 26 cells. A, temporal accumulation of *TfR1* mRNA in Colon 26 cells after 50% serum shock. The data are normalized using β-*actin* as a control. Points, mean (n = 3, P < 0.01, ANOVA); bars, SEM. Data are plotted relative to the 0-h value after 50% serum shock. B, temporal accumulation of c-MYC protein in control cells or c-Myc knockdown cells after 50% serum shock. Colon 26 cells were transfected with scrambled siRNA (control siRNA) or specific siRNA for c-Myc (c-Myc siRNA). Crude cell extracts were measured by Western blotting analysis. The data were normalized using β-actin as a control. Points, mean (n = 3, control cells; P < 0.01, ANOVA); bars, SEM. *; P < 0.05, when compared with the value for the control siRNA group at the corresponding times. C, temporal accumulation of *TfR1* mRNA in control cells or *c-Myc* knockdown cells. The mRNA levels of *TfR1* were determined at the indicated time points after serum treatment. Points, mean (n = 3, control cells; P < 0.01, ANOVA); bars, SEM. *, P < 0.05, when compared with the value for the control siRNA group at the corresponding times.

cells (Fig. 4A). The results of chromatin immunoprecipitation analysis revealed that endogenous c-MYC in Colon 26 cells bound to the E-box element in the intron region of *TfR1* gene (Fig. 4B). Of particular note, the binding amounts of c-MYC increasedat the time of day corresponding to the peak of *TfR1* mRNA expression (see Fig. 1B), suggesting that the time-dependent binding of c-MYC to the E-box in *TfR1* gene underlies its rhythmic expression. In addition, the mRNA levels of a prototypical c-MYC–regulated gene, telomerase reverse transcriptase (23), in Colon 26 cells implanted in mice also showed time-dependent variation (Supplementary Data S5).

Relationship between the rhythmic expression of TfR1 and time dependency of Pt incorporation into tumor DNA

Tf-NGPE L-OHP is a transferrin-conjugated liposome encapsulating L-OHP, a diaminocyclohexane Pt antitumor agent, which forms adducts with DNA. Tf-NGPE L-OHP binds to TfR, which is expressed on the plasma membrane and can internalize Pt into the cell.[3] Thus, to explore the function of internalization into the cell through transferrin in the rhythmic expression of TfR1, we investigated the temporal profile of *TfR1* gene expression and incorporation of Pt into tumor DNA in synchronized and desynchronized Colon 26 cells. A brief exposure of cultured Colon 26 cells to 50% FBS medium for 2 hours induced an oscillation in the expression of *TfR1* mRNA (Fig. 5A). The mRNA levels of *TfR1* peaked at 18 hours after treatment of the cells with 50% FBS. The oscillation of *TfR1* mRNA levels was also found on day 3 after serum treatment (see Fig. 3). The amount of Pt incorporated into the DNA of serum-shocked cells after treatment with Tf-NGPE L-OHP increased significantly at the time point corresponding to the peak in the level of TfR1 protein (P < 0.05; Fig. 5B). In contrast, in nontreated cells, neither the mRNA and protein levels of TfR1 nor Pt incorporation showed significant time-dependent variations (Fig. 5A and B), suggesting that the oscillation in the

[3] Our unpublished data.

Published OnlineFirst July 14, 2010; DOI:10.1158/0008-5472.CAN-10-0184

expression of TfR1 underlies the time-dependent change in Pt incorporation into tumor DNA.

Influence of dosing time on the ability of Tf-NGPE L-OHP to inhibit tumor growth

The plasma Pt concentration decreased gradually after a single injection of 7.5 mg/kg Tf-NGPE L-OHP (i.v.) at both dosing times, but the Pt concentration in plasma at 3 hours after Tf-NGPE L-OHP injection was significantly higher in mice injected with the drug at 9:00 a.m. than at 9:00 p.m. (Fig. 6A, left). On the other hand, Pt incorporation into DNA in tumor cells at 3 and 6 hours after Tf-NGPE L-OHP injection was significantly higher in mice injected with the drug at 9:00 p.m. than at 9:00 a.m. (Fig. 6A, right). We also attempted to determine the Pt contents in tumor DNA at over 6 hours after Tf-NGPE L-OHP injection, but accurate assessment was difficult, probably due to L-OHP–induced apoptotic or necrotic tumor cell death.

A significant antitumor effect of Tf-NGPE L-OHP was observed when tumor-bearing mice were injected i.v. with a single dose of 7.5 mg/kg L-OHP (Supplementary Data S3). Thus, the dosage was set at 7.5 mg/kg to investigate whether the antitumor effect of Tf-NGPE L-OHP was altered depending on its dosing time. The growth of tumor cells was significantly suppressed by the administration of Tf-NGPE L-OHP (7.5 mg/kg, i.v.). The antitumor effects were more potent in mice injected with the drug at 9:00 p.m. than in those that received it at 9:00 a.m. (Fig. 6B). Fifteen days after injection of the drug, the tumor volume in mice injected with Tf-NGPE L-OHP at 9:00 p.m. was significantly smaller than that in mice injected at 9:00 a.m. ($P < 0.05$).

Discussion

TfR1 is a key cell surface molecule that regulates the uptake of iron-bound transferrin (8). It has been shown that correlation exists between the number of surface TfR1 and the rate of cell proliferation. TfR1 expression is higher in tumor cells than in normal cells. Thus, intracellular targeting using iron-saturated Tf as a ligand for TfR-mediated endocytosis has attracted attention. In this study, the protein abundance of TfR1 on Colon 26 tumor cells implanted in mice showed a clear 24-hour oscillation. The rhythmic phase of TfR1 protein

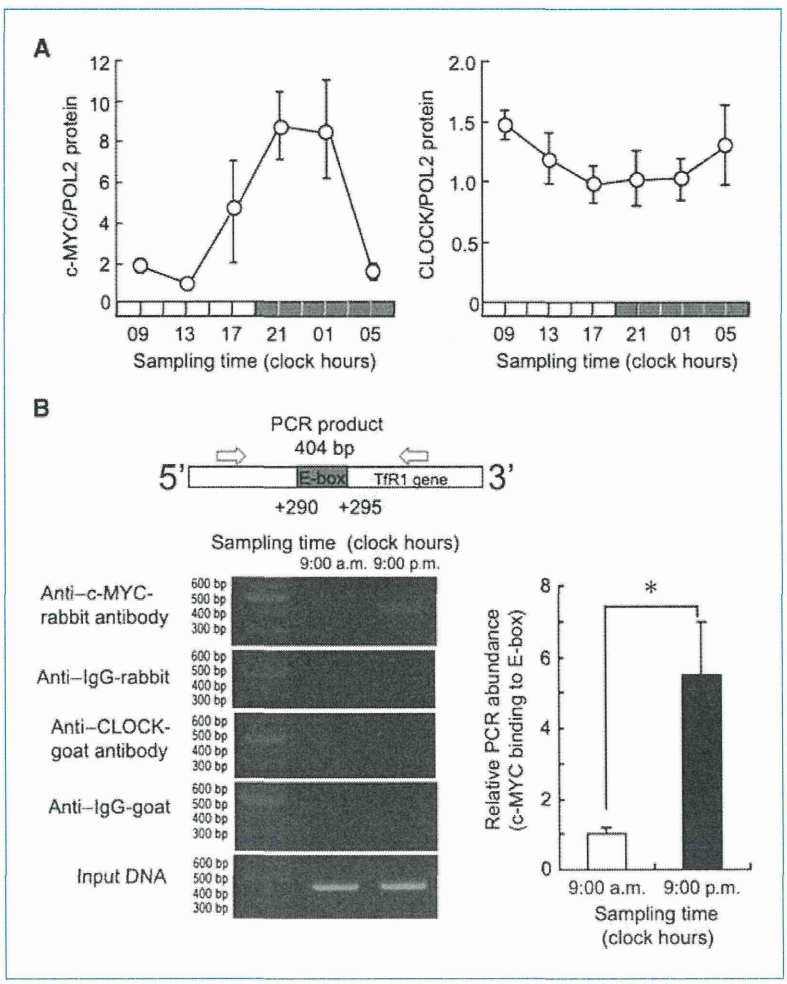

Figure 4. Time-dependent changes in the binding of endogenous c-MYC to the E-box element in the *TfR1* gene. A, temporal expression profiles of protein levels of c-MYC and CLOCK in implanted Colon 26 tumor masses. POL2 protein was used as an internal control whose expression was constant throughout the day. The data are normalized using POL2 as a control ($P < 0.01$, ANOVA). CLOCK protein did not show an obvious variation. Points, mean ($n = 3$); bars, SEM. B, left, temporal profiles of the binding of endogenous c-MYC to the *TfR1* gene in Colon 26 cells implanted in mice. Right, the quantification of temporal changes in the binding of c-MYC to the *TfR1* gene in Colon 26 cells implanted in mice. The mean value of each assay at 9:00 a.m. was set at 1. Columns, mean ($n = 3$); bars, SEM. *; $P < 0.05$ for the comparison between the two groups.

Published OnlineFirst July 14, 2010; DOI:10.1158/0008-5472.CAN-10-0184

paralleled that of its mRNA levels. However, the mechanisms of transcriptional rhythm of TfR1 were unclear.

The molecular circadian clock operates at a cellular level and coordinates a wide variety of physiologic processes (24). CLOCK/BMAL1 heterodimers activate the transcription of *Per, Cry,* and *Dec* genes through CACGTG E-box enhancer elements (8). The results of luciferase reporter assays and chromatin immunoprecipitation experiments revealed that the CACGTG E-box located in the first intron of the mouse *TfR1* gene was unable to respond to CLOCK/BMAL1 heterodimers. In contrast, as reported previously (19), c-MYC could bind to the E-box of the mouse *TfR1* gene and activate its transcription. The amount of endogenous c-MYC protein binding to the mouse *TfR1* gene E-box fluctuated in a time-dependent manner. The binding of c-MYC to the E-box increased at the time corresponding to the peak of *TfR1* mRNA expression, suggesting that c-MYC acts as a regulator of circadian expression of the *TfR1* gene in Colon 26 tumor cells. This hypothesis was also supported by the present findings that the amplitude of the *TfR1* mRNA rhythm in serum-shocked Colon 26 cells was decreased by the down-regulation of c-MYC. On the other hand, CLOCK protein did not bind to the *TfR1* gene E-box. This may account for the unresponsiveness of the *TfR1* gene to CLOCK/BMAL1 heterodimers. The sequence surrounding the E-box and its location had a marked influence on the transcriptional activity of CLOCK/BMAL1 (6). In fact, a CT-rich *cis*-acting element of the mouse vasopressin gene confers robust CLOCK/BMAL1 responsiveness on an adjacent E-box (25). The absence of such a CT-rich *cis*-acting element around the E-box may result in the inability of CLOCK/BMAL1 to transactivate the mouse *TfR1* gene.

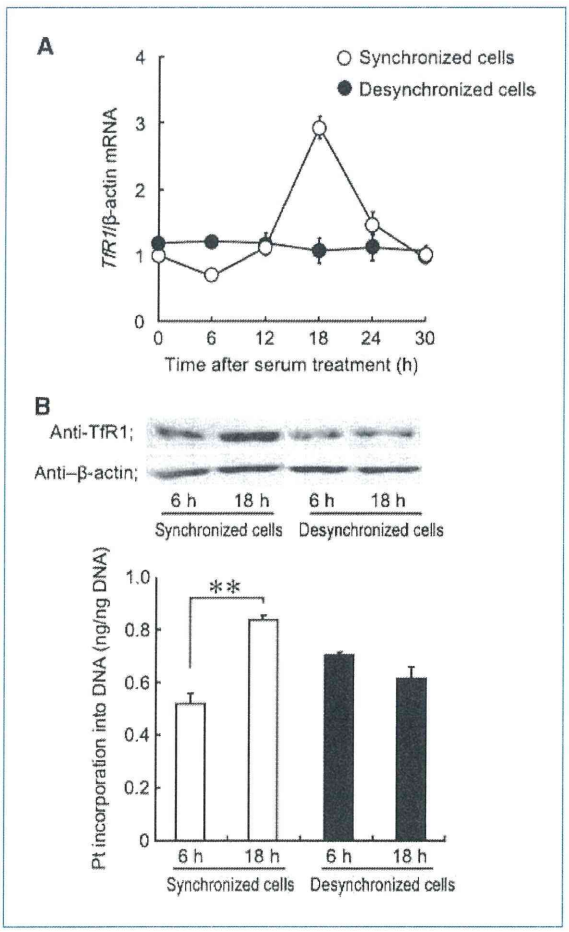

Figure 5. Influence of rhythmic changes in the expression of TfR1 on intratumoral delivery of L-OHP by Tf-NGPE liposomes. A, the temporal expression profile of *TfR1* mRNA in synchronized (○) or unsynchronized (●) Colon 26 cells. Cultured Colon 26 cells were synchronized by exposure to 50% FBS for 2 h. Points, mean ($n = 3$, synchronized cells; $P < 0.05$, ANOVA); bars, SEM. B, the photographs show temporal expression of TfR1 protein in synchronized or unsynchronized Colon 26 cells. Bottom, that temporal profile of Pt incorporation into DNA in synchronized or unsynchronized Colon 26 cells. Cells were exposed to Tf-NGPE L-OHP (L-OHP: 0.4 mg/mL) for 3 h at 6 or 18 h after the serum treatment, and then the amounts of Pt incorporated into tumor DNA were measured. Columns, mean ($n = 3$); bars, SEM. *, $P < 0.05$ for the comparison between the two time points.

It was reported previously that L-OHP could accumulate in tumor masses following delivery using Tf-PEG liposomes (16). TfR-targeting liposomes also bind to TfR on tumor cell surfaces and are internalized into the cells by receptor-mediated endocytosis. In this study, to evaluate the function of the 24-hour oscillation in TfR1, Tf-NGPE liposomes were used as a targeting carrier for intratumoral delivery of L-OHP. This TfR-targeting liposomal DDS exhibited similar pharmacokinetic properties to Tf-PEG liposomes, and i.v. administration of L-OHP encapsulated within Tf-NGPE liposomes lead to the accumulation of a high concentration of L-OHP in tumors as much as Tf-PEG liposomes.[4] The amount of Pt in tumor DNA after Tf-NGPE L-OHP injection increased at the times of day when TfR1 was abundant on the tumor surface in this study. This notion was also supported by *in vitro* findings that the time dependency of Tf-NGPE liposome–delivered L-OHP into tumor cells disappeared in the absence of the oscillation in TfR1 expression. These findings suggest that the oscillation in the expression of TfR1 underlies the dosing time–dependent changes in the internalization into

[4] Our unpublished data.

Published OnlineFirst July 14, 2010; DOI:10.1158/0008-5472.CAN-10-0184

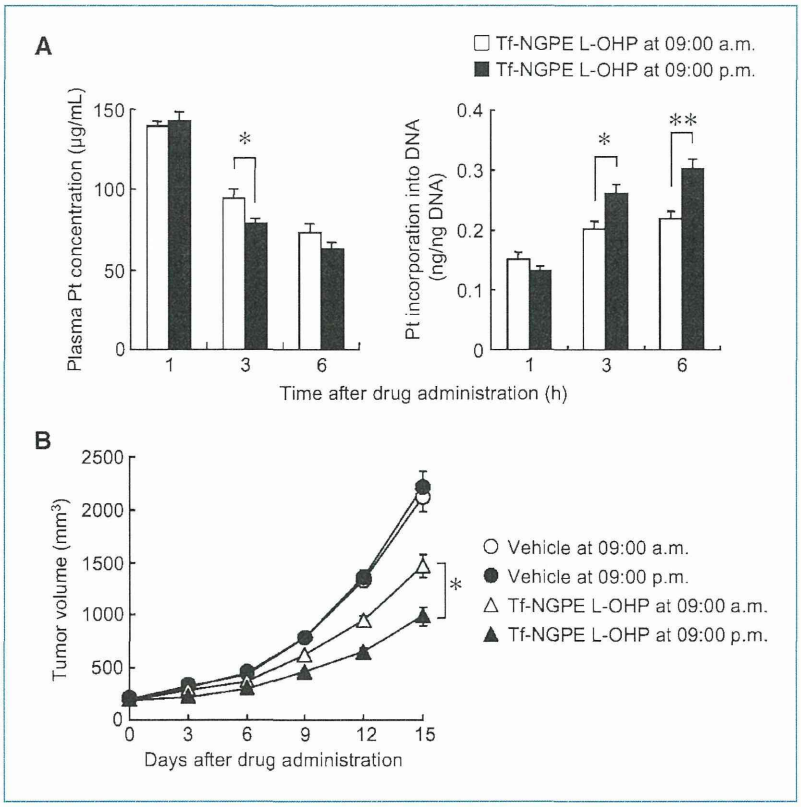

Figure 6. Influence of dosing time on the ability of Tf-PEG L-OHP to inhibit tumor growth in mice. Colon 26 tumor–bearing mice were injected i.v. with a single dose of Tf-NGPE L-OHP (L-OHP: 7.5 mg/kg) or vehicle (9% sucrose) at 9:00 a.m. or 9:00 p.m. A, dosing time–dependent differences in the intratumoral delivery of L-OHP by Tf-NGPE liposomes were examined. Plasma Pt concentration (left) and Pt incorporation into tumor DNA (right) were measured at the indicated times after an injection of Tf-NGPE L-OHP. Columns, mean (n = 5); bars, SEM; **, $P < 0.01$; *, $P < 0.05$ for comparison between the two groups. B, dosing time–dependent difference in the antitumor effect of Tf-NGPE L-OHP. Points, mean (n = 8–10); bars, SEM; *, $P < 0.05$ for comparison between the two dosing times.

the cells by receptor-mediated endocytosis. In addition, after a single injection of Tf-NGPE L-OHP, the antitumor effect of the drug varied according to its dosing time. The dosing time dependency of the antitumor effect seemed to be caused by time-dependent changes in the intratumoral delivery of L-OHP by TfR-targeting liposomes.

In the present study, it was shown that the 24-hour rhythm of TfR1 expression in colon cancer cells was controlled by c-MYC, and the cyclical accumulation of TfR1 caused dosing time–dependent changes in the intratumoral delivery of L-OHP by receptor-mediated endocytosis. Identification of the circadian properties of molecules that are targeted by ligand-directed DDS may aid the choice of the most appropriate time of day for their administration.

Disclosure of Potential Conflicts of Interest

The authors disclose no conflicts.

Grant Support

Grants-in-Aid for Scientific Research on Priority Areas "Cancer" (S.O. 20014016) from the Ministry of Education, Culture, Sport, Science and Technology of Japan, for Scientific Research (B; S.O. 21390047), for Challenging Exploratory Research (S.O. 21659041), and for the Encouragement of Young Scientists (N.M. 20790137) from the Japan Society for the Promotion of Science.

The costs of publication of this article were defrayed in part by the payment of page charges. This article must therefore be hereby marked *advertisement* in accordance with 18 U.S.C. Section 1734 solely to indicate this fact.

Received 01/18/2010; revised 06/07/2010; accepted 06/07/2010; published OnlineFirst 07/14/2010.

References

1. Stephan FK, Zucker I. Circadian rhythms in drinking behavior and locomotor activity of rats are eliminated by hypothalamic lesions. Proc Natl Acad Sci U S A 1972;69:1583–6.
2. Alvarez JD, Sehgal A. Circadian rhythms: finer clock control. Nature 2002;419:798–9.
3. Gekakis N, Staknis D, Nguyen HB, et al. Role of the CLOCK protein in the mammalian circadian mechanism. Science 1998;280:1564–9.
4. Kume K, Zylka MJ, Sriram S, et al. mCRY1 and mCRY2 are essential components of the negative limb of the circadian clock feedback loop. Cell 1999;98:193–205.
5. Preitner N, Damiola F, Lopez-Molina L, et al. The orphan nuclear receptor REV-ERBα controls circadian transcription within the positive limb of the mammalian circadian oscillator. Cell 2002;110:251–60.
6. Sato TK, Yamada RG, Ukai H, et al. Feedback repression is required for mammalian circadian clock function. Nat Genet 2006;38:312–9.

Published OnlineFirst July 14, 2010; DOI:10.1158/0008-5472.CAN-10-0184

7. Koyanagi S, Kuramoto Y, Nakagawa H, et al. A molecular mechanism regulating circadian expression of vascular endothelial growth factor in tumor cells. Cancer Res 2003;63:7277–83.
8. Daniels TR, Delgado T, Helguera G, Penichet ML. The transferrin receptor part II: targeted delivery of therapeutic agents into cancer cells. Clin Immunol 2006;121:159–76.
9. Sorokin LM, Morgan EH, Yeoh GC. Transformation-induced changes in transferrin and iron metabolism in myogenic cells. Cancer Res 1989;49:1941–7.
10. Niitsu Y, Kohgo Y, Nishisato T, et al. Transferrin receptors in human cancerous tissues. Tohoku J Exp Med 1987;153:239–43.
11. Calzolari A, Oliviero I, Deaglio S, et al. Transferrin receptor 2 is frequently expressed in human cancer cell lines. Blood Cells Mol Dis 2007;39:82–91.
12. Kawabata H, Nakamaki T, Ikonomi P, Smith RD, Germain RS, Koeffler HP. Expression of transferrin receptor 2 in normal and neoplastic hematopoietic cells. Blood 2001;98:2714–9.
13. Röhrs S, Kutzner N, Vlad A, Grunwald T, Ziegler S, Müller O. Chronological expression of Wnt target genes Ccnd1, Myc, Cdkn1a, TfRc, Plf1 and Ramp3. Cell Biol Int 2009;33:501–8.
14. Papahadjopoulos D, Allen TM, Gabizon A, et al. Sterically stabilized liposomes: improvements in pharmacokinetics and antitumor therapeutic efficacy. Proc Natl Acad Sci U S A 1991;88:11460–4.
15. Ishida O, Maruyama K, Tanahashi H, et al. Liposomes bearing polyethyleneglycol-coupled transferrin with intracellular targeting property to the solid tumors *in vivo*. Pharm Res 2001;18:1042–8.
16. Suzuki R, Takizawa T, Kuwata Y, et al. Effective anti-tumor activity of oxaliplatin encapsulated in transferrin-PEG-liposome. Int J Pharm 2008;346:143–50.
17. Ohdo S, Koyanagi S, Suyama H, Higuchi S, Aramaki H. Changing the dosing schedule minimizes the disruptive effects of interferon on clock function. Nat Med 2001;3:356–60.
18. Holloway K, Sade H, Romero IA, Male D. Action of transcription factors in the control of transferrin receptor expression in human brain endothelium. J Mol Biol 2007;365:1271–84.
19. O'Donnell KA, Yu D, Zeller KI, et al. Activation of transferrin receptor 1 by c-Myc enhances cellular proliferation and tumorigenesis. Mol. Cell Biol 2006;26:2373–86.
20. Oishi K, Miyazaki K, Kadota K, et al. Genome-wide expression analysis of mouse liver reveals CLOCK-regulated circadian output genes. J Biol Chem 2003;278:41519–27.
21. Takiguchi T, Tomita M, Matsunaga N, Nakagawa H, Koyanagi S, Ohdo S. Molecular basis for rhythmic expression of CYP3A4 in serum-shocked HepG2 cells. Pharmacogenet Genomics 2007;17:1047–56.
22. Wittekindt NE, Hörtnagel K, Geltinger C, Polack A. Activation of c-*myc* promoter P1 by immunoglobulin κ gene enhancers in Burkitt lymphoma: functional characterization of the intron enhancer motifs κB, E box 1 and E box 2, and of the 3′ enhancer motif PU. Nucleic Acids Res 2000;28:800–8.
23. Reymann S, Borlak J. Transcription profiling of lung adenocarcinomas of c-*myc*-transgenic mice: identification of the c-*myc* regulatory gene network. BMC Syst Biol 2008;2:46.
24. Weaver ReppertSM. Coordination of circadian timing in mammals. Nature 2002;418:935–41.
25. Muñoz E, Brewer M, Baler R. Modulation of BMAL/CLOCK/E-Box complex activity by a CT-rich *cis*-acting element. Mol Cell Endocrinol 2006;252:74–81.
26. Fu L, Pelicano H, Liu J, Huang P, Lee C. The circadian gene Period2 plays an important role in tumor suppression and DNA damage response *in vivo*. Cell 2002;111:41–50.

Biomaterials 31 (2010) 7813–7826

Contents lists available at ScienceDirect

Biomaterials

journal homepage: www.elsevier.com/locate/biomaterials

Development of an ultrasound-responsive and mannose-modified gene carrier for DNA vaccine therapy

Keita Un [a,b], Shigeru Kawakami [a], Ryo Suzuki [c], Kazuo Maruyama [c], Fumiyoshi Yamashita [a], Mitsuru Hashida [a,d,*]

[a] Department of Drug Delivery Research, Graduate School of Pharmaceutical Sciences, Kyoto University, 46-29 Yoshida-shimoadachi-cho, Sakyo-ku, Kyoto 606-8501, Japan
[b] The Japan Society for the Promotion of Science (JSPS), Chiyoda-ku, Tokyo 102-8471, Japan
[c] Department of Biopharmaceutics, School of Pharmaceutical Sciences, Teikyo University, 1091-1 Suwarashi, Sagamiko, Sagamihara, Kanagawa 229-0195, Japan
[d] Institute for Integrated Cell-Material Sciences (iCeMS), Kyoto University, Yoshida-ushinomiya-cho, Sakyo-ku, Kyoto 606-8302, Japan

ARTICLE INFO

Article history:
Received 31 May 2010
Accepted 29 June 2010
Available online 24 July 2010

Keywords:
Gene transfer
Bubble lipoplexes
Ultrasound exposure
Mannose receptors
Antigen presenting cells
DNA vaccine therapy

ABSTRACT

Development of a gene delivery system to transfer the gene of interest selectively and efficiently into targeted cells is essential for achievement of sufficient therapeutic effects by gene therapy. Here, we succeeded in developing the gene transfection method using ultrasound (US)-responsive and mannose-modified gene carriers, named Man-PEG_{2000} bubble lipoplexes. Compared with the conventional lipofection method using mannose-modified carriers, this transfection method using Man-PEG_{2000} bubble lipoplexes and US exposure enabled approximately 500~800-fold higher gene expressions in the antigen presenting cells (APCs) selectively in vivo. This enhanced gene expression was contributed by the improvement of delivering efficiency of nucleic acids to the targeted organs, and by the increase of introducing efficiency of nucleic acids into the cytoplasm followed by US exposure. Moreover, high anti-tumor effects were demonstrated by applying this method to DNA vaccine therapy using ovalbumin (OVA)-expressing plasmid DNA (pDNA). This US-responsive and cell-specific gene delivery system can be widely applied to medical treatments such as vaccine therapy and anti-inflammation therapy, which its targeted cells are APCs, and our findings may help in establishing innovative methods for in-vivo gene delivery to overcome the poor introducing efficiency of carriers into cytoplasm which the major obstacle associated with gene delivery by non-viral carriers.

1. Introduction

In the post-genome era, the analysis of disease-related genes has rapidly advanced, and the medical application of the information obtained from gene analysis is being put into practice. In particular, the development of effective method to transfer the gene of interest selectively and efficiently into the targeted cells is essential for the gene therapy of refractory diseases, in-vivo functional analysis of genes and establishment of animal models for diseases. However, a suitable carrier for selective and efficient gene transfer to the targeted cells is still being developed. Although various types of viral and non-viral carriers have been developed for gene transfer, they are limited to use by viral-associated pathogenesis and low transfection efficiency, respectively. For the cell-selective gene transfer, many investigators have focused on ligand-modified non-viral carriers such as liposomes [1–4], emulsions [5], micelles [6] and polymers [7], because of their high productivity and low toxicity. On the other hand, since the gene transfection efficiency by non-viral carriers is poor, it is difficult to obtain the effective therapeutic effects by gene therapy using non-viral carriers. Moreover, in the gene transfection using conventional ligand-modified non-viral carriers, since the carriers need to be taken up into cells via endocytosis following by interaction with targeted molecules on the cell membrane, the number of candidates which are suitable as ligands for targeted gene delivery is limited.

Some researchers have attempted to develop the transfection method using external stimulation, such as electrical energy [8], physical pressure [9] and water pressure [10], to enhance the gene transfection efficiency. Among these, gene transfection method using US exposure and microbubbles enclosing US imaging gas, called "sonoporation method", have been focused as effective drug/gene delivery systems [11–14]. In the sonoporation method, microbubbles are degraded by US exposure with optimized intensity, then cavitation energy is generated by the destruction of

* Corresponding author. Department of Drug Delivery Research, Graduate School of Pharmaceutical Sciences, Kyoto University, 46-29 Yoshida-shimoadachi-cho, Sakyo-ku, Kyoto 606-8501, Japan. Tel.: +81 75 753 4545; fax: +81 75 753 4575.
E-mail address: hashidam@pharm.kyoto-u.ac.jp (M. Hashida).

0142-9612/$ – see front matter © 2010 Elsevier Ltd. All rights reserved.
doi:10.1016/j.biomaterials.2010.06.058

microbubbles. Consequently, the transient pores are created on the cell membrane, and large amount of nucleic acids are directly introduced into the cytoplasm through the created pores [13,15,16]. However, the in-vivo gene transfection efficiency by conventional sonoporation method administering the nucleic acids and microbubbles separately is low because of the rapid degradation of nucleic acids in the body [17], the large particle size of conventional microbubbles [15] and the different pharmacokinetic profiles of the nucleic acids and microbubbles. Moreover, to transfer the gene into the targeted cells selectively by sonoporation method in vivo, the control of in-vivo distribution of nucleic acids and microbubbles, which are separately administered, is necessary.

In our previous report [16], we have demonstrated the effective transfection by combination-use method using our mannosylated lipoplexes composed of Man-C4-chol: DOPE [1], and conventional Bubble liposomes (BLs) [12] with US exposure. However, this combination-use method is complicated because of the necessity for multiple injections of mannosylated lipoplexes and BLs; therefore, it is difficult to apply for medical treatments using multiple transfections. In addition, the difference of in-vivo distribution characteristics between mannosylated lipoplexes and BLs might be decreased its transfection efficacy. Therefore, it is essential to develop the US-responsive and cell-selective gene carriers constructed with ligand-modified gene carriers and microbubbles.

Taking these into considerations, we examined the gene transfection system for effective DNA vaccine therapy using physical stimulation and ligand-modification. First, we developed US-responsive and mannose-modified gene carriers, Man-PEG_{2000} bubble lipoplexes (Fig. 1), by enclosing perfluoropropane gas into mannose-conjugated PEG_{2000}-DSPE-modified cationic liposomes (DSTAP: DSPC: Man-PEG_{2000}-DSPE (Fig. 1))/pDNA complexes. Then, we evaluated the enhanced and cell-selective gene expression in the APCs by intravenous administration of Man-PEG_{2000} bubble lipoplexes and external US exposure in mice. Finally, we examined high anti-tumor effects by applying this method to DNA vaccine therapy using OVA-expressing pDNA.

2. Materials and methods

2.1. Mice and cell lines

Female ICR mice (4~5 weeks old) and C57BL/6 mice (6~8 weeks old) were purchased from the Shizuoka Agricultural Cooperative Association for Laboratory Animals (Shizuoka, Japan). All animal experiments were carried out in accordance with the Principles of Laboratory Animal Care as adopted and promulgated by the US National Institutes of Health and the guideline for animal experiments of Kyoto University. CD8-OVA1.3 cells, T cell hybridomas with specificity for OVA 257~264-kb, were kindly provided by Dr. C.V. Harding (Case Western Reserve University, Cleveland, OH, USA) [18]. EL4 cells (C57BL/6 T-lymphomas) and E.G7-OVA cells (the OVA-transfected clones of EL4) were purchased from American Type Culture Collection (Manassas, VA). CD8-OVA1.3 cells and EL4 cells were maintained in Dulbecco's modified Eagle's medium and E.G7-OVA cells were maintained in RPMI-1640. Both mediums were supplemented with 10% fetal bovine serum (FBS), 0.05 mM 2-mercaptoethanol, 100 IU/mL penicillin, 100 μg/mL streptomycin and 2 mM L-glutamine at 37 °C in 5% CO_2.

2.2. pDNA

pCMV-Luc and pCMV-OVA were constructed in our previous reports [19,20]. Briefly, pCMV-Luc was constructed by subcloning the HindIII/Xba I firefly luciferase cDNA fragment from pGL3-control vector (Promega, Madison, WI, USA) into the polylinker of pcDNA3 vector (Invitrogen, Carlsbad, CA, USA). pCMV-OVA was constructed by subcloning the EcoRI chicken egg albumin (ovalbumin) cDNA fragment from pAc-neo-OVA, which was kindly provided by Dr. M.J. Bevan (University of Washington, Seattle, WA, USA) into the polylinker of pVAX I. pDNA were amplified in the E. coli strain DH5α, isolated and purified using a QIAGEN Endofree Plasmid Giga Kit (QIAGEN GmbH, Hilden, Germany).

2.3. Synthesis of Man-PEG_{2000}-DSPE and preparation of Man-PEG_{2000} bubble lipoplexes

Man-PEG_{2000}-DSPE was synthesized in a one-step reaction by covalent binding with NH_2-PEG_{2000}-DSPE (NOF Co., Tokyo, Japan) and 2-imino-2-methoxyethyl-1-thiomannoside (IME-thiomannoside). IME-thiomannoside was prepared according to the method of Lee [21]. Next, NH_2-PEG_{2000}-DSPE and IME-thiomannoside were reacted, vacuum dried and dialyzed to produce Man-PEG_{2000}-DSPE, and then, the resultant dialysates were lyophilized. To produce the liposomes for bubble lipoplexes, DSTAP (Avanti Polar Lipids Inc., Alabaster, AL, USA), DSPC (Sigma Chemicals Inc., St. Louis, MO, USA) and Man-PEG_{2000}-DSPE or NH_2-PEG_{2000}-DSPE were mixed in chloroform at a molar ratio of 7:2:1. For construction of BLs, DSPC and methoxy-PEG_{2000}-DSPE (NOF Co., Tokyo, Japan) were mixed in chloroform at a molar ratio of 94:6. The mixture for the construction of liposomes was dried by evaporation, vacuum desiccated and the resultant lipid film was resuspended in sterile 5% dextrose. After hydration for 30 min at 65 °C, the dispersion was sonicated for 10 min in a bath sonicator and for 3 min in a tip sonicator to produce liposomes. Then, liposomes were sterilized by passage through a 0.45 μm filter (Nihon-Millipore, Tokyo, Japan). The lipoplexes were prepared by gently mixing with equal volumes of pDNA and liposome solution at a charge ratio of 1.0:2.3 (−:+). For preparation of BLs and bubble lipoplexes, the enclosure of US imaging gas into liposomes and lipoplexes was performed according to our previous report [16]. Briefly, prepared liposomes and lipoplexes were added to 5 mL sterilized vials, filled with perfluoropropane gas (Takachiho Chemical Industries Co., Ltd., Tokyo, Japan), capped and then pressured with 7.5 mL of perfluoropropane gas. To enclose US imaging gas into the liposomes and lipoplexes, the vial was sonicated using a bath-type sonicator (AS ONE Co., Osaka, Japan) for 5 min. The particle sizes and zeta

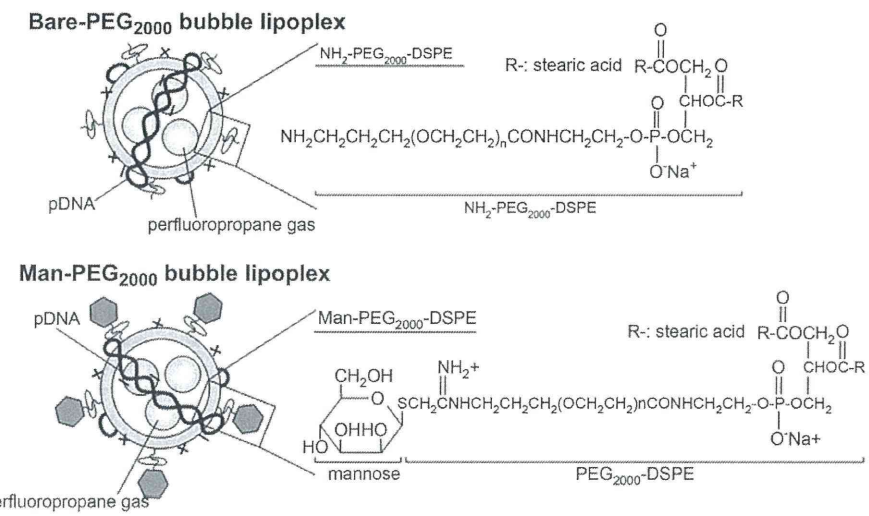

Fig. 1. Structure of Bare-PEG_{2000} bubble lipoplex containing NH_2-PEG_{2000}-DSPE and Man-PEG_{2000} bubble lipoplex containing Man-PEG_{2000}-DSPE used in this study.

potentials of liposomes and lipoplexes were determined by a Zetasizer Nano ZS instrument (Malvern Instrument, Ltd., Worcestershire, UK).

2.4. Harvesting of mouse peritoneal macrophages

Mouse peritoneal macrophages were harvested and cultured according to our previous report [16]. Briefly, the macrophages were harvested from mice at 4 days after intraperitoneal injection of 2.9% thioglycolate medium (1 mL). The collected macrophages were washed and suspended in RPMI-1640 medium supplemented with 10% FBS, 100 IU/mL penicillin, 100 μg/mL streptomycin and 2 mM L-glutamine, and plated on culture plates. After incubation for 2 h at 37 °C in 5% CO_2, non-adherent cells were washed off with culture medium, and the macrophages were incubated for another 72 h.

2.5. In-vitro gene transfection

After the macrophages were collected and incubated for 72 h, the culture medium was replaced with Opti-MEM I containing bubble lipoplexes (5 μg pDNA). The macrophages were exposed to US (frequency, 2.062 MHz; duty, 50%; burst rate, 10 Hz; intensity 4.0 W/cm^2) for 20 s using a 6 mm diameter probe placed in the well at 5 min after addition of bubble lipoplexes. In the transfection using naked pDNA and BLs, at 5 min after addition of naked pDNA (5 μg) and BLs (60 μg total lipids) were added, and the macrophages were immediately exposed to US. US was generated using a Sonopore-4000 sonicator (NEPA GENE, Chiba, Japan). Then, 1 h later, the incubation medium was replaced with RPMI-1640 and incubated for an additional 23 h. Lipofectamine® 2000 (Invitrogen, Carlsbad, CA, USA) was used according to the recommended procedures, and the exposure time of Lipofectamine® 2000 was 1 h, which is the same exposure time in other experiments using lipoplexes. Following incubation for 24 h, the cells were scraped from the plates and suspended in lysis buffer (0.05% Triton X-100, 2 mM EDTA, 0.1 M Tris, pH 7.8). Then, the cell suspension was shaken, and centrifuged at 10,000*g*, 4 °C for 10 min. The supernatant was mixed with luciferase assay buffer (Picagene, Toyo Ink Co., Ltd., Tokyo, Japan) and the luciferase activity was measured in a luminometer (Lumat LB 9507, EG&G Berthold, Bad Wildbad, Germany). The luciferase activity was normalized with respect to the protein content of cells. The protein concentration was determined with a Protein Quantification Kit (Dojindo Molecular Technologies, Inc., Tokyo, Japan). The level of luciferase mRNA expression was determined by RT-PCR.

2.6. Inhibitory experiments of endocytosis in vitro

Endocytosis was inhibited by chlorpromazine (50 μM) as clathrin-mediated endocytosis inhibitor [22], genistein (200 μM) as caveolae-mediated endocytosis inhibitor [23] and 5-(*N*-ethyl-*N*-isopropyl)amiloride (EIPA, 50 μM) as macropinocytosis inhibitor [24]. Each endocytosis inhibitor was added to the macrophages at 30 min before the addition of lipoplexes.

2.7. Fluorescence photographs of pDNA in mouse peritoneal macrophages

To visualize the cellular association of pDNA by fluorescence microscopy (Biozero BZ-8000, KEYENCE, Osaka, Japan), lipoplexes were constructed with TM-rhodamine-labeled pDNA prepared by a Label IT Nucleic Acid Labeling Kit (Mirus Co., Madison, WI, USA).

2.8. Evaluation of cytotoxic effects by MTT assay

The cytotoxicity was evaluated by MTT assay. Briefly, 3-(4,5-dimethyl-2-thiazol)-2,5-diphenyltetrazolium bromide (MTT, Nacalai Tesque, Inc., Kyoto, Japan) solution was added to each well and incubated for 4 h. The resultant formazan crystals were dissolved in 0.04 M HCl-isopropanol and sonicated for 10 min in a bath sonicator. Absorbance values at 550 nm (test wavelength) and 655 nm (reference wavelength) were measured and the results were expressed as viability (%).

2.9. In-vivo gene transfection

Four-week-old ICR female mice were intravenously injected with 400 μL bubble lipoplexes via the tail vein using a 26-gauge syringe needle at a dose of 50 μg pDNA. At 5 min after the injection of bubble lipoplexes, US (frequency, 1.045 MHz; duty, 50%; burst rate, 10 Hz; intensity 1.0 W/cm^2; time, 2 min) was exposed transdermally to the abdominal area using a Sonopore-4000 sonicator with a probe of diameter 20 mm. In the transfection using naked pDNA and BLs, at 4 min after intravenous injection of BLs (500 μg total lipid), naked pDNA (50 μg) was intravenously injected and US was exposed at 1 min after naked pDNA injection. At predetermined times after injection, mice were sacrificed and their organs collected for each experiment. The organs were washed twice with cold saline and homogenized with lysis buffer (0.05% Triton X-100, 2 mM EDTA, 0.1 M Tris, pH 7.8). The lysis buffer was added in a weight ratio of 5 mL/*g* for the liver or 4 mL/*g* for the other organs. After three cycles of freezing and thawing, the homogenates were centrifuged at 10,000*g*, 4 °C for 10 min. The luciferase activity of resultant supernatant was determined by luciferase assay and the level of luciferase mRNA expression was determined by RT-PCR.

2.10. In-vivo imaging

At 6 h after transfection, anesthetized mice were administrated D-luciferin (10 mg/300 μL PBS) (Promega Co., Madison, WI, USA). At 10 min after injection of D-luciferin, organs were excised and luminescent images were taken by NightOWL LB 981 NC instrument (Berthold Technologies, GmbH, Bad Wildbad, Germany). The pseudocolor luminescent images were generated, overlaid with organ images and the luminescence representation was obtained using WinLight software (Berthold Technologies GmbH, Bad Wildbad, Germany).

2.11. Separation of mouse hepatic PCs and NPCs

The separation of mouse hepatic PCs and NPCs was performed according to our previous reports [19]. Briefly, at 6 h after in-vivo transfection using bubble lipoplexes and US exposure, each mouse was anesthetized with pentobarbital sodium (40~60 mg/kg) and the liver was perfused with perfusion buffer (Ca^{2+}, Mg^{2+}-free HEPES solution, pH 7.2) for 10 min. Then, the liver was perfused with collagenase buffer (HEPES solution, pH 7.5 containing 5 mM $CaCl_2$ and 0.05% (w/v) collagenase (type I)) for 5 min. Immediately after the start of perfusion, the vena cava and aorta were cut and the perfusion rate was maintained at 5 mL/min. At the end of perfusion, the liver was excised. The cells were dispersed in ice-cold Hank's-HEPES buffer by gentle stirring and then filtered through cotton mesh sieves, followed by centrifugation at 50*g* for 1 min. The pellets containing the hepatic PCs were washed five times with Hank's-HEPES buffer by centrifuging at 50*g* for 1 min. The supernatant containing the hepatic NPCs was similarly centrifuged 5 times and the resulting supernatant was centrifuged twice at 300*g* for 10 min. Then, the PCs and NPCs were resuspended separately in ice-cold Hank's-HEPES buffer.

2.12. Isolation of mouse splenic CD11c$^+$ cells

The isolation of mouse splenic CD11c$^+$ cells was performed according to our previous reports [25]. Briefly, At 6 h after in-vivo transfection using bubble lipoplexes and US exposure, the splenic cells were suspended in ice-cold RPMI-1640 medium on ice. Red blood cells were removed by incubation with hemolytic reagent (0.15 M NH_4Cl, 10 mM $KHCO_3$, 0.1 mM EDTA) for 3 min at room temperature. The CD11c$^+$ cells were isolated by magnetic cell sorting with anti-mouse CD11c (N418) microbeads and auto MACS (Miltenyi Biotec, Inc., Auburn, CA, USA) following the manufacturer's instructions.

2.13. Quantitative RT-PCR

Total RNA was isolated from separated cells using a GenElute Mammalian Total RNA Miniprep Kit (Sigma-Aldrich, St. Louis, MO, USA). Reverse transcription of mRNA was carried out using a PrimeScript® RT reagent Kit (Takara Bio Inc., Shiga, Japan). Real-time PCR was performed using SYBR® Premix Ex Taq (Takara Bio Inc., Shiga, Japan) and Lightcycler Quick System 350S (Roche Diagnostics, Indianapolis, IN, USA) with primers. The primers for luciferase and gapdh cDNA were constructed as follows: primer for luciferase cDNA, 5′-TTCTTCGCCAAAAGCACTC-3′ (forward) and 5′-CCCTCGGGTGTAATCAGAAT-3′ (reverse); primer for gapdh, 5′-TCTCCTGCGACTTCAACA-3′ (forward) and 5′-GCTGTAGCCGTATTCATTGT-3′ (reverse) (Sigma-Aldrich, St. Louis, MO, USA). The mRNA copy numbers were calculated for each sample from the standard curve using the instrument software ('Arithmetic Fit Point analysis' for the Lightcycler). The results were expressed as the ratio of luciferase mRNA copy numbers to the housekeeping gene (gapdh) mRNA copy numbers.

2.14. Tissue distribution of radio-labeled pDNA

Lipoplexes constructed with ^{32}P-labeled pDNA ([α-^{32}P]-dCTP, PerkinElmer, Inc., MA, USA) [26] were injected intravenously into mice. At predetermined times after injection, blood was collected from the vena cava under pentobarbital anesthesia. Then, mice were sacrificed and the organs were collected, rinsed with saline and weighed. The tissues were dissolved in Soluene-350 and the resultant lysates were decolorized with isopropanol and 30% H_2O_2, and then neutralized with 5 N HCl. The radioactivity of ^{32}P-labeled pDNA was measured in scintillation counter (LSA-500, Beckman Coulter, Inc., CA, USA) after addition of Clear-Sol I solution.

2.15. Measurement of transaminase activity in the serum

At predetermined times after transfection, the serum was collected from the anesthetized mice. Alanine aminotransferase (ALT) and aspartate aminotransferase (AST) activities in the serum were determined using Transaminase CII-Test Wako kit (Wako Pure Chemical Industries Ltd., Tokyo, Japan) according to manufacturer's instructions.